Backscattering reduction in a sharply bent water wave channel

S. Kucher,[1] A. Koźluk,[1,2] P. Petitjeans,[1] A. Maurel,[3] and V. Pagneux[4,*]

[1]*Laboratoire de Physique et Mécanique des Milieux Hétérogènes, UMR CNRS 7636, ESPCI-Paris, Université PSL, Sorbonne Université, Université Paris Cité, 75005 Paris, France*

[2]*Institute of Aeronautics and Applied Mechanics, Warsaw University of Technology, 00-665 Warsaw, Poland*

[3]*Institut Langevin, UMR CNRS 7587, ESPCI-Paris, 75005 Paris, France*

[4]*Laboratoire d'Acoustique de l'Université du Mans, UMR CNRS 6613, 72085 Le Mans, France*

(Received 3 August 2023; revised 11 November 2023; accepted 17 November 2023; published 18 December 2023)

We study theoretically and experimentally how to reduce the backscattering of water waves in a channel with multiple turns. We show that it is possible not only to cancel backscattering but also to achieve a remarkable transmission in such geometries. In order to avoid the reflection that naturally arises at each turn of the waveguide, an anisotropic metamaterial made of closely spaced thin vertical plates is used. The efficiency of the metamaterial arrangement depends only slightly on the frequency of the incident wave, as long as its wavelength is much larger than the periodicity of the array. This phenomenon is applies not only to water wave channels but also to any type of waves with Neumann boundary conditions.

DOI: 10.1103/PhysRevB.108.214311

I. INTRODUCTION

The use of metamaterials for wave manipulation has generated considerable interest in recent years, both in electromagnetics and in acoustics and surface waves [1–4]. Metamaterials typically consist of a periodic structure whose characteristic length is much smaller than the considered wavelength and allow us to modify the natural propagation of waves. They are able to generate, for example, invisibility cloaking [5–7], wave absorption [8–11], or wave shifting [12–15], among other effects.

In particular, in the context of water waves, one type of metamaterial commonly used to control wave propagation is an array of rigid plates forming a subwavelength grating. Systems of this type have been studied both experimentally [13,16] and theoretically [17–20]. They have been found to possess Brewster-angle-type behavior, in which backscattering is considerably reduced and near-zero reflection values are achieved for a wide range of frequencies [21–24], without relying on resonant phenomena. When it is not zero reflection for a wide frequency band that is sought, but rather the objective is the stability of transparency with changing angle, note that wide-angle transparent anisotropic metamaterials have been proposed for electromagnetic waves [25,26].

In order to facilitate the modeling of the properties of gratings with a subwavelength structure, homogenization techniques have been developed [16,23,24,27,28]. These techniques replace the perforated domain with a homogeneous and anisotropic one. At low enough frequencies, under the homogenization regime approximation, they are capable of accurately predicting the behavior of the system, with the decrease in backscattering at the Brewster angle. If the plates constituting the grating occupy the entire depth of the fluid, going from the bottom to the surface, since the space between them is smaller than the incident wavelength, the energy flow is forced in one direction only. Of particular interest is the recent work of Porter [17], who showed that if the thickness of the plates is infinitely thin, then the reflection is exactly zero (i.e., without making use of the homogenization regime approximation).

Naturally, there has been an interest in performing experiments on shifting waves using a subwavelength grating. For example, reflectionless waveguides with an angle up to $\pi/6$ have been achieved for water waves [13], using the theory of transformation media to design a metabathymetry with anisotropic properties. In the context of acoustics, a beam shifter capable of exhibiting a high transmission at resonant frequencies and at a Brewster-like incidence angle has been realized [15].

In this paper, we show theoretically and experimentally a broadband backscattering reduction in a sharply bent water wave channel. This is achieved owing to an array of vertical surface-piercing thin plates with a perpendicular angle with respect to the incident wave, as shown in Fig. 1. The effect is broadband because the spacing between the plates is much smaller than the incident wavelength, resulting in an effective medium without impedance mismatch between the inside and the outside. The paper is organized as follows. In Sec. II we characterize the reflection generated by the bending of a waveguide. The use of a plate-array metamaterial to reduce the backscattering after each turn is proposed in Sec. III. We study the reflection coefficient given by a plane wave incidence on a plate-array grating both in an infinite domain and in a bent waveguide. We also propose a homogenized model to replace the subwavelength grating by an effective medium. Finally, in Sec. IV we show an experimental realization of this system, exploring its capabilities in terms of frequency.

*Corresponding author: vincent.pagneux@univ-lemans.fr

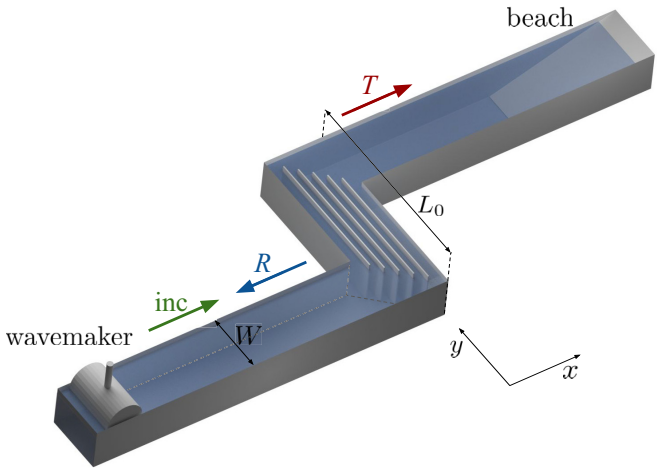

FIG. 1. Scheme of the experimental setup: a channel of width W with a dislocation of length L_0, where the plate-array metamaterial is placed. An incident wave (inc) is reflected and transmitted with scattering coefficients R and T.

II. SHARPLY BENT WATER WAVE CHANNEL

The system under consideration is depicted in Fig. 1. Surface waves are generated at the beginning of the channel, which undergoes a perpendicular turn of length L_0 and then continues in a direction parallel to the first section. At the end of the channel an absorbing beach avoids reflections. We first consider this geometry without metamaterial to characterize the amount of reflection it generates. Thereafter we will show, in the next section, that it is possible to reduce the backscattering generated by the turn by adding a plate-array metamaterial in the central region that allows high values of transmission to be achieved as well.

The free-surface elevation $\eta(x, y)$ with time harmonic dependence $e^{-i\omega t}$ is governed by the two-dimensional (2D) Helmholtz equation

$$(\Delta + k^2)\eta(x, y) = 0, \tag{1}$$

where k is the wave number, along with Neumann boundary conditions on the vertical walls $\partial_n \eta = 0$. This equation is valid for irrotational and incompressible flows in geometries with a flat bottom and vertical walls in the harmonic regime, under the linear approximation.

We consider waves that are generated for frequencies below the cutoff frequency of the waveguide of width W, i.e., $kW < \pi$, which only allows the propagation of the planar mode. Under the wide-spacing approximation, it is then possible to construct a 1D model that takes into account the scattering coefficients of each perpendicular turn individually, along with 1D propagation following the waveguide (see Appendix A). It can be noticed that this system is analogous to a Fabry-Pérot interferometer, in which waves pass through a cavity made up of two parallel reflecting surfaces separated by a distance $L = L_0 - W$. Following this 1D model, the absolute value of the reflection coefficient of the bent channel is given by

$$|R|^2 = \frac{F \sin^2\left(\frac{\delta}{2}\right)}{1 + F \sin^2\left(\frac{\delta}{2}\right)}, \tag{2}$$

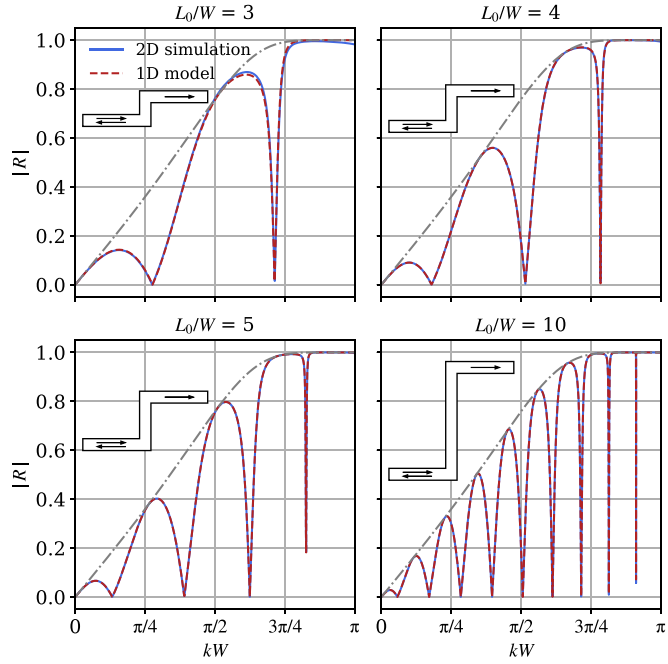

FIG. 2. Reflection coefficient for different ratios of L_0/W without the metamaterial. The solid blue curves exhibit the result of a 2D simulation of the full channel, the dashed red curves indicate the Fabry-Pérot resonances, and the dash-dotted gray curves show the envelope of $|R|$, obtained from Eq. (2).

defining $F = 4r_0^2/(1 - r_0^2)^2$ and $\delta = 2kL + 2\varphi$, where r_0 and φ are the modulus and the phase, respectively, of the reflection coefficient ($r = r_0 e^{i\varphi}$) for one single perpendicular turn (see Appendix B).

Clearly, backscattering suppression is achieved when $\sin^2(\delta/2) = 0$, i.e., when $kL + \varphi = m\pi$ ($m \in \mathbb{Z}$). Additionally, the envelope of this expression can be obtained by imposing $\sin^2(\delta/2) = 1$ and is given by $|R|^2 = F/(1 + F)$, which depends only on r_0. We may note that the absolute value of the reflection coefficient for one corner yields the shape of the envelope, while its phase provides the position of the resonances, as we will see in Fig. 2.

In order to study the dependence of the reflection coefficient R on the distance L_0 of the perpendicular turn, Fig. 2 shows the values of $|R|$, for different ratios of L_0/W, obtained from the 1D model [Eq. (2)] as well as the ones computed numerically by solving Eq. (1) in the full 2D geometry using the finite-element method (MATLAB PDETOOL). There are two behaviors that are worth noting when the ratio L_0/W is increased. Firstly, the number of resonances becomes consequently higher, as expected from Eq. (2). Secondly, the 1D model agrees very well with the full 2D simulation, and unsurprisingly under the wide-spacing approximation, this agreement gets better and better when the two perpendicular corners move away from each other since the near-field effects decrease.

Regardless of the L_0/W ratio, the general tendency of the reflection coefficient is the same. It is zero at resonance frequencies, while its upper envelope $\sqrt{F/(1+F)}$ does not depend on L_0/W. In the following, we will add a plate-array

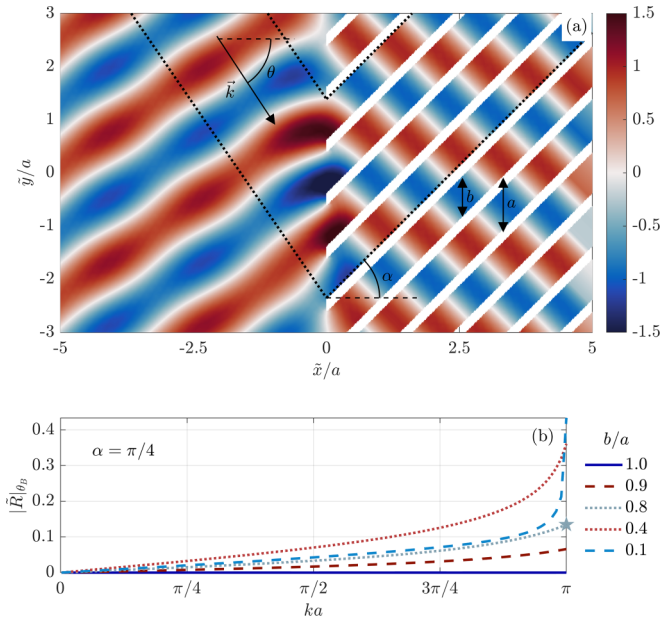

FIG. 3. (a) Real part of the surface elevation field $\eta(x, y)$ for a plane wave incidence with wave number k and incident angle θ over a semi-infinite array of tilted plates with a periodicity a and inclination angle $\alpha = \pi/4$. b is the spacing between the plates. Here, $b/a = 0.8$, $ka = \pi$, and $\theta = \theta_B$. The dotted lines indicate where the channel walls would be if we confined this system as in Fig. 1. (b) Reflection coefficient as a function of ka for this geometry with $\alpha = \pi/4$, for different values of the filling ratio b/a, for a plane wave incidence at the Brewster angle θ_B [Eq. (3)]. The star indicates the point that corresponds to the surface shown in (a).

metamaterial in order to reduce the backscattering of the turn, and without loss of generality, we will work at $L_0/W = 3.2$.

III. PLATE-ARRAY METAMATERIAL

With the aim of reducing the reflection that naturally arises at the turn, we are going to use an anisotropic metamaterial that significantly diminishes the reflection at each turn. The metamaterial consists of an array of thin parallel and closely spaced plates of length $L = L_0 - W$ vertically placed in the central region, as shown in Fig. 1. The vertical plates are surface piercing, spanning from the channel bottom to above the fluid surface.

A. Reflection on an infinite grating

First, to assess the reflection reduction capabilities, it is necessary to determine the characteristics of the plate-array metamaterial, namely, the thickness of the plates and the spacing between them. In order to understand the effect of the plate thickness on the scattered fields, we begin by considering the problem of a plane wave incidence on an infinite periodic grating made of parallel inclined plates, as shown in Fig. 3. The periodic array is composed of plates with periodicity a separated by a distance b, making an angle α with respect to the $\tilde{x}$ axis [29]. We consider a plane wave incidence with incident angle θ: For $ka \leqslant \pi$, no higher-order modes can propagate, and there is only reflection with coefficient $\tilde{R}(k, \theta)$ at the specular angle by the grating.

If the wavelength is much smaller than the periodicity of the array, such that $ka \ll 1$, the hypothesis of the homogenization regime is satisfied. In this case, it is possible to obtain a Brewster-like behavior, i.e., a zero of reflection for an incidence angle θ_B given by

$$\theta_B = \cos^{-1}\left(\frac{b}{a}\cos\alpha\right), \tag{3}$$

in agreement with previous works [23]. It is worth mentioning that when the plates have no inclination ($\alpha = 0$), we recover the expression for the Brewster angle as it is usually found for subwavelength gratings [27].

Since we use the approximation $ka \ll 1$ to obtain the expression for θ_B [Eq. (3)], it is expected that the reflection is not exactly zero. We examine then the exact reflection of a plane wave at the Brewster angle θ_B, for different values of the filling ratio of water, b/a. Results are displayed in Fig. 3 for the case of $\alpha = \pi/4$. We utilized COMSOL MULTIPHYSICS to conduct these numerical simulations. In Fig. 3(a) an example of the solution for $b/a = 0.8$ is presented; even at the Brewster angle, there is a small amount of reflection, due to the deviation from the homogenization theory. To get a quantitative evaluation of these small reflection values at the Brewster angle, Fig. 3(b) illustrates the absolute value of the reflection coefficient $|\tilde{R}|_{\theta_B}$ obtained for various configurations, changing the thickness of the plates. As expected, $|\tilde{R}|_{\theta_B}$ increases with ka. However, surprisingly, this trend is not monotonous with b/a, with a maximum around $b/a \approx 0.4$. Incidentally, we verified that this tendency is independent of the value of α.

The case where $b = a$ is of particular interest because it corresponds to exactly zero reflection up to $ka = \pi$ for the Brewster angle. This property can be explained by two arguments [23]: (i) the invisibility of infinitesimally thin plates when $\vec{k}$ is parallel to the plates and (ii) the reciprocity implying $\tilde{R}(\theta) = \tilde{R}(-\theta)$. In the following, we will work with the thinnest plates achievable (since a zero thickness is unattainable in an experimental setup). Moreover, the angle $\alpha = \pi/4$ that we have considered in the results yields a right angle between the incident and transmitted waves for the Brewster case, which corresponds to a turn of $\pi/2$ in the bent waveguide.

B. Reflection on a grating in the bent waveguide

Bringing our focus back to the primary objective, i.e., to reduce the backscattering in a sharply bent water wave channel, we consider plates with a finite thickness d, and we confine the system into a waveguide of width W with two perpendicular turns, each turn being constructed as indicated with dotted lines in Fig. 3(a). Since we are going to perform experiments, we chose the thickness of the plates to be $d = 0.02W$ so that the reflection is minimized and the plates are rigid enough. Now the reflection is not exactly zero for two reasons: Firstly, the plates have a nonzero thickness, and secondly, there are edge effects because the channel walls stop the periodicity. The case of infinitesimally thin plates in a waveguide is considered in Appendix C to illustrate these edge effects. In the

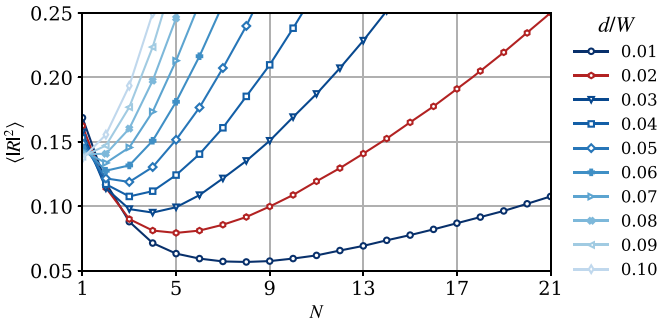

FIG. 4. Mean (over all the frequencies below f_{cutoff}) of the absolute value of the reflection coefficient as a function of the number of plates for different values of thickness. The thickness that we chose to perform experiments is indicated in red.

following, we will evaluate the impact of the plate thickness on $|R|$.

We performed numerical simulations taking a number N of plates and computing the mean value of $|R|^2$ over all the frequencies below f_{cutoff}, for different values of thickness $d/W \in [0.01, 0.10]$. The obtained curves are shown in Fig. 4. We can observe that, as expected, the mean reflection diminishes with the plate thickness. The number of plates also plays a role in the reflection coefficient. For a small number of plates, the hypothesis $ka \ll 1$ is not satisfied, while for a large value of N, the high density of plates creates a barrier within the channel. There is therefore an optimal number of plates for each thickness for which the minimum of $|R|$ is achieved. For the chosen value $d/W = 0.02$ (red curve in Fig. 4), the optimal number of plates is $N = 5$. In this case, despite having nonzero-thickness plates (rigid enough), the reflection coefficient is globally (broadband in frequency) small, not so far from the ideal case of zero-thickness plates for an infinite grating discussed in the previous section.

C. Homogenized model

As stated previously, the plate-array metamaterial only allows 1D propagation in the direction of the plates, since the periodicity of the array is much smaller than the wavelength. It has been shown that, under this approximation, the periodic structure yields the same wave properties as an effective medium obtained through homogenization theory [23,28]. Then, the plate-array metamaterial can be replaced by a homogeneous anisotropic medium, and the homogenized wave equation takes the form

$$\text{div}\mathbf{U} + \phi k^2 \eta(x, y) = 0, \quad \mathbf{U} = \begin{pmatrix} 0 & 0 \\ 0 & \phi \end{pmatrix} \nabla \eta(x, y), \tag{4}$$

with η and $\mathbf{U} \cdot \mathbf{n}$ being continuous at the interfaces between the channel and the effective medium, and where ϕ is the filling ratio of water, given by

$$\phi = 1 - Nd/W. \tag{5}$$

$\phi = 0$ corresponds to the entire channel filled with plates, while $\phi = 1$ corresponds to plates with zero thickness.

In order to get more insight into the modeling of the behavior of the system, we are going to compare 2D numerical

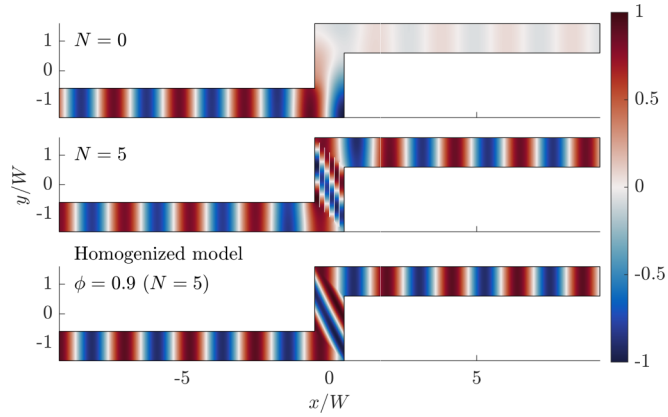

FIG. 5. Numerical result: real part of the simulated field at $kW = 9\pi/10$ for an empty channel, a channel with five vertical plates in the middle region, and a homogenized medium with the filling ratio corresponding to $N = 5$.

simulations of the channel with the plate-array metamaterial with the homogenization results. To illustrate this comparison, Fig. 5 shows the free-surface deformation field obtained numerically for a fixed frequency for the channel in three different configurations: without the metamaterial, with a metamaterial made up of $N = 5$ vertical plates, and the corresponding effective medium with $\phi = 0.9$. We observe that, as already mentioned, there is a very high reflection in the absence of the metamaterial, while the backscattering is considerably reduced when the plates or the effective medium are added. We also note a very good agreement between the homogenized model and the real geometry (as also shown in Appendix B). This agreement improves as the system approaches the solution of an infinite array of infinitesimally thin plates, i.e., by increasing the number of plates and decreasing their thickness.

The filling ratio of water can be adjusted by changing either the thickness of the plates or their quantity. In this study, the plate thickness is fixed at $d/W = 0.02$, as it strikes a balance between minimizing backscattering and enabling practical experiments. Therefore we varied the number of plates N to modify the filling ratio. The reflection coefficient was then computed at various frequencies for different values of N, as illustrated in Fig. 6. The reflection coefficient obtained from the homogenized model is also depicted in the same figure, with the corresponding value of ϕ for each N, related by Eq. (5).

In Fig. 6 we can observe that, in the absence of plates ($N = 0$), $|R|$ increases with the frequency and exhibits Fabry-Pérot resonance, as seen in Fig. 2. Surprisingly and interestingly, the addition of only one plate already changes drastically the behavior of $|R|$, resulting in low reflection values across all frequencies, except at the resonances. In that case, of course, the effective medium does not describe the system accurately. The reflection coefficient obtained from the homogenized model converges to the one from the actual problem as the number of plates increases. It is worth mentioning that the results of the 2D simulations with plates were used to average across all frequencies and obtain the data points presented in Fig. 4.

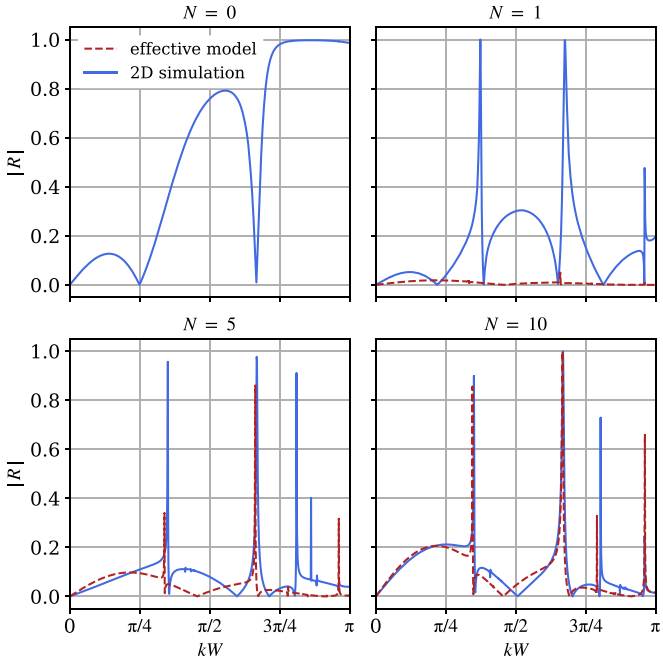

FIG. 6. Reflection coefficient for different numbers of plates with a fixed thickness of $d = 0.02W$ (solid blue curves) and the one obtained from the effective model with the corresponding value of the filling ratio (dashed red curves).

IV. EXPERIMENTAL RESULTS

Experiments were performed in a 2.95-m-long channel of width $W = 0.10$ m, with a turn of $L_0 = 0.32$ m and a constant water level of $h = 0.05$ m. Waves are generated at one side of the channel by a wave maker for frequencies in the range $f \in [1.0, 2.7]$ Hz, with a 0.05-Hz step ($f_{\text{cutoff}} = 2.69$ Hz). The frequency is linked to the wave number k through the dispersion relation of gravity-capillarity waves

$$\omega^2 = \left(gk + \frac{\sigma}{\rho}k^3\right)\tanh kh, \tag{6}$$

where $\omega = 2\pi f$, g is the gravity acceleration, $\rho = 1000$ kg/m^3 and $\sigma = 71$ mN/m are the water density and surface tension, respectively. This equation is only used to link the frequency ω imposed by the wave maker with its corresponding number k.

The wave maker is driven by a linear motor that generates a sinusoidal vertical movement with an amplitude of 2 mm. This amplitude has been checked to be low enough to remain in the linear regime. On the other side of the channel we placed an absorbing beach inclined at 5° in order to reduce spurious reflections from the outgoing region. Measurements were taken using the Fourier transform profilometry method [30,31], which allows single-shot measurements of the whole free surface. A sinusoidal (reference) pattern is projected on the free surface of the liquid, and this projection is filmed from above. We used distilled water with a small amount of TiO_2 (4 g/L) in order to be able to project on its surface; it has been shown that this concentration does not modify significantly the hydrodynamical properties of water [32]. The phase of the projected pattern is modified by the deformations of the free surface; the difference between this deformed phase and the reference one allows for the reconstruction of the height field. Two identical systems consisting of a video projector (Epson EH-TW9400) and a USB camera (Basler acA1920-155um) arranged in a parallel-axis geometry were mounted and synchronized at each side of the perpendicular turn. We took measurements of the full width of the channel, 1.12 m at each side of the turn, at 30 frames/s.

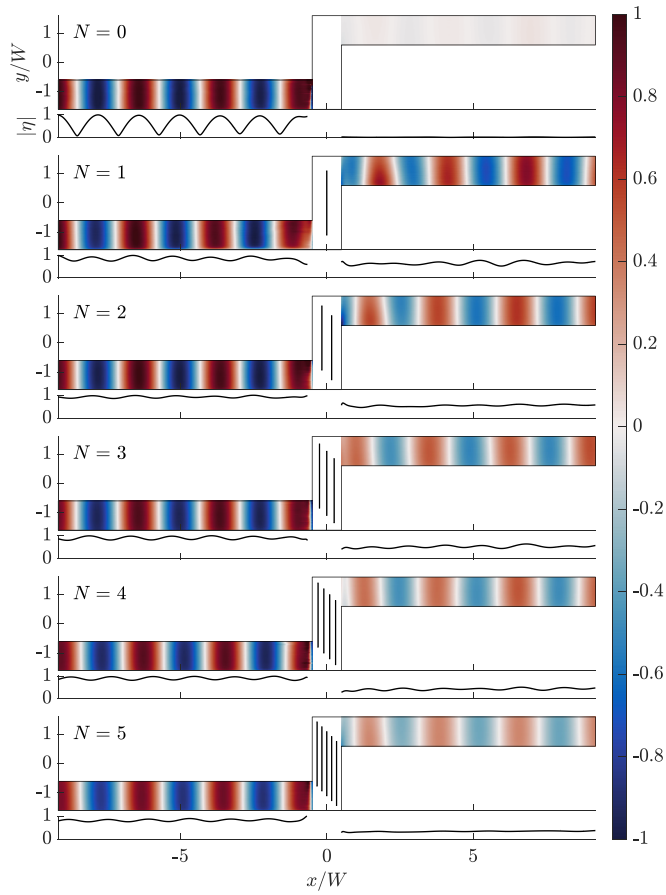

FIG. 7. Experimental result: real part (top graph in each panel) and average of the absolute value (bottom graph in each panel) of the measured free-surface deformation filtered at the forcing frequency for $kW = 9\pi/10$ (normalized).

We investigated experimentally the effect of the filling ratio, changing the number of plates with a fixed thickness of $d = 2$ mm. Figure 7 shows the height fields at $kW = 9\pi/10$ for different numbers of plates between $N = 0$ ($\phi = 1$) and $N = 5$ ($\phi = 0.90$). In the absence of metamaterial, the transmission is close to zero, while in its presence the transmission increases considerably. As mentioned earlier with the numerical results, it is worth noting that the addition of only one plate has already a remarkable effect.

To obtain a more comprehensive understanding than can be gained at just a single frequency, we subsequently explored the broadband character of the backscattering reduction. In order to extract the reflection and transmission coefficients, we filtered the height field at the forcing frequency and averaged it in the y direction: $\eta(x) = \langle \eta(x, y) \rangle_y$. Then, since only the

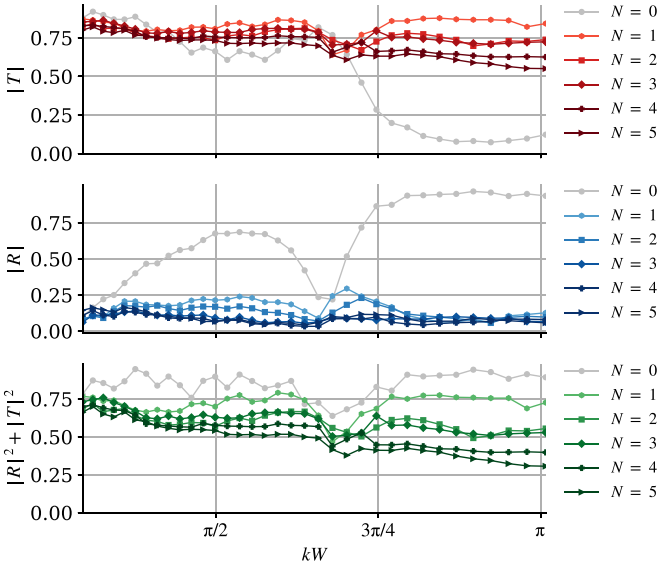

FIG. 8. Reflection and transmission coefficients obtained experimentally for different numbers of plates.

plane mode is propagating, η can be written as

$$\eta(x) = \begin{cases} A(e^{ikx} + Re^{-ikx}), & \text{in region I} \\ ATe^{ikx}, & \text{in region II,} \end{cases} \tag{7}$$

where A is the amplitude of the incident wave, R and T are the reflection and transmission coefficients, and regions I and II correspond to the far field before and after the turn (i.e., for $x < 0$ and $x > 0$), respectively. Figure 8 shows the reflection and transmission coefficients as well as the energy for 35 different frequencies, obtained by performing a fit on each side with Eq. (7) [33]. For the measurement with $N = 0$ (gray curve), we recover the behavior of the reflection and transmission coefficients predicted numerically as well as the Fabry-Pérot resonance, which disappears almost completely with the addition of the plates. Besides, we note that the scattered energy flux decreases as the number of plates increases for all frequencies. This is due to losses in the experiment that were not considered in the numerical approach. If we consider only viscous losses given by the bulk viscosity and the bottom and wall friction, the theory [34–36] predicts much lower dissipation than the one observed in the experiment (Fig. 8). Therefore we can reasonably assess that this dissipation is generated mostly by meniscus effects. Consequently, the optimal number of plates does not match the one found numerically, since the transmission past the turn diminishes with the number of plates. However, even in the cases where high transmission is not entirely achieved, the plate array reduces the backscattering significantly.

With a detailed inspection of Fig. 8, we can distinguish several behaviors: The plate-array metamaterial can yield high transmission, low reflection, or both, depending on the parameters chosen (filling ratio and frequency). When adding the metamaterial, the reflection drops drastically and takes values lower than 30% for all tested configurations, becoming progressively smaller as the number of plates increases. Nevertheless, due to the viscous losses, an experimental minimum of reflection does not necessarily correspond to a maximum of transmission. Indeed, the maximum of transmission occurs when $N = 1$; this case is of particular interest especially for high frequencies, where, as it turns out, adding as few as only one plate is enough to considerably increase the transmission through the turns.

V. CONCLUDING REMARKS

We designed and built an experimental plate-array metamaterial capable of reducing the backscattering of surface waves in a sharply bent waveguide for a broadband range of frequencies without relying on resonant phenomena. Essentially, the role of the metamaterial is to reduce the reflection by impedance matching, and in a lossless case, this implies automatically a high transmission. In an experimental realization, a high attenuation due to viscous friction might be anticipated since the plates are closely spaced. However, by fine-tuning the number of plates, we have shown that this device not only reduces the backscattering but also allows for a remarkable transmission. Surprisingly, even using only one plate provides already a very strong reduction of backscattering and a good transmission. It is important to point out that the broadband backscattering reduction can be achieved for turns in channels with angles other than $\pi/2$, where it can lead to the construction of more complex devices, e.g., with several successive turns.

ACKNOWLEDGMENTS

S.K., P.P., A.M., and V.P. acknowledge the support of the Agence Nationale de la Recherche (ANR) under Grant No. 243560 CoProMM.

APPENDIX A: 1D MODEL

We consider the problem of a plane wave within the time harmonic regime that passes through two refractive interfaces separated by a distance L. When the incident wave reaches the first interface, there is a reflected wave and a transmitted wave. The latter is then reflected and transmitted at the second interface. The reflected wave coming from the second interface arrives again at the first one, and this process continues an infinite number of times. Therefore it is necessary to consider the infinite sum of reflected and transmitted waves. Eventually, after infinite reflections, a stationary solution consisting

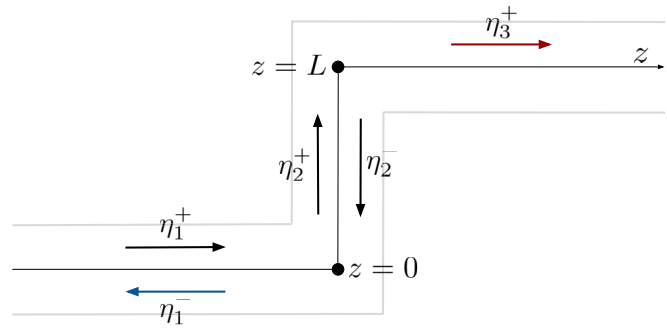

FIG. 9. Propagative waves established in the stationary solution for a 1D problem with two reflective interfaces.

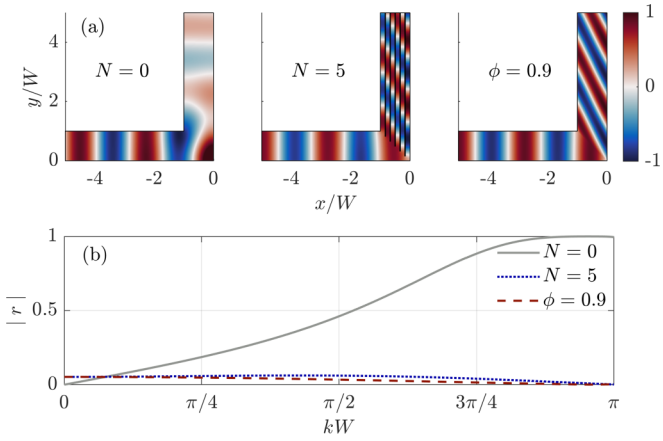

FIG. 10. Numerical result. (a) Real part of the simulated field at $kW = 9\pi/10$ for an incident wave reaching one perpendicular turn with no plates, five vertical plates, and a homogenized medium with the filling ratio corresponding to $N = 5$. (b) Absolute value of the reflection coefficient for the above configurations.

of five propagating wave components is established, as shown in Fig. 9.

These five waves can be expressed as

$$\begin{aligned}
\eta_1^+(z) &= A_1 e^{ikz},\\
\eta_1^-(z) &= B_1 e^{-ikz},\\
\eta_2^+(z) &= A_2 e^{ikz},\\
\eta_2^-(z) &= B_2 e^{-ikz},\\
\eta_3^+(z) &= A_3 e^{ikz},
\end{aligned} \tag{A1}$$

where A_1 is known and where $A_1, A_2, A_3, B_1, B_2 \in \mathbb{C}$ and can be obtained from the matching conditions at $z = 0$ and $z = L$. We will express these waves as a function of the reflection and transmission coefficients of the interfaces, r and t, supposed to be symmetric and the same for both the reflected wave and the transmitted wave.

$$\begin{aligned}
\eta_2^+(z=0) &= t\eta_1^+(z=0) + r\eta_2^+(z=0),\\
\eta_1^-(z=0) &= r\eta_1^+(z=0) + t\eta_2^-(z=0),\\
\eta_2^-(z=L) &= r\eta_2^+(z=L),\\
\eta_3^+(z=L) &= t\eta_2^+(z=L).
\end{aligned} \tag{A2}$$

Evaluating the expressions at $z = 0$ and $z = L$, we obtain

$$\begin{aligned}
A_2 &= tA_1 + rB_1,\\
B_1 &= rA_1 + tB_2,\\
B_2 e^{-ikL} &= rA_2 e^{ikL},\\
A_3 e^{ikL} &= tA_2 e^{ikL}.
\end{aligned} \tag{A3}$$

The amplitude of the outgoing wave η_3^+ can be expressed as

$$A_3 = \frac{t^2 A_1}{1 - r^2 e^{2ikL}}. \tag{A4}$$

This expression allows us to calculate the transmission as

$$|T|^2 = \frac{|A_3|^2}{|A_1|^2} = \frac{|t|^4}{|1 - r^2 e^{2ikL}|^2}. \tag{A5}$$

Noting $r = r_0 e^{i\varphi}$ (with $r_0 = |r|$) and using the property $|r|^2 + |t|^2 = 1$, we can write $|T|^2$ as

$$|T|^2 = \frac{1}{1 + F\sin^2\left(\frac{\delta}{2}\right)}, \tag{A6}$$

where $F = 4r_0^2/(1 - r_0^2)^2$ and $\delta = 2kL + 2\varphi$. This equation depends on the absolute value of the reflection coefficient r_0 and its phase φ, as well as the distance L between the interfaces. Since $|R|^2 + |T|^2 = 1$, we can easily obtain the reflection coefficient:

$$|R|^2 = \frac{F\sin^2\left(\frac{\delta}{2}\right)}{1 + F\sin^2\left(\frac{\delta}{2}\right)}. \tag{A7}$$

APPENDIX B: ONE CORNER

We consider an incident plane wave with harmonic time dependence propagating in a waveguide of width W and reaching one perpendicular turn. We consider frequencies below the cutoff frequency, i.e., $kW < \pi$, where only the planar mode can propagate. We performed numerical simulations in order to find the reflection coefficient r for this system. Three different configurations were considered: an empty channel,

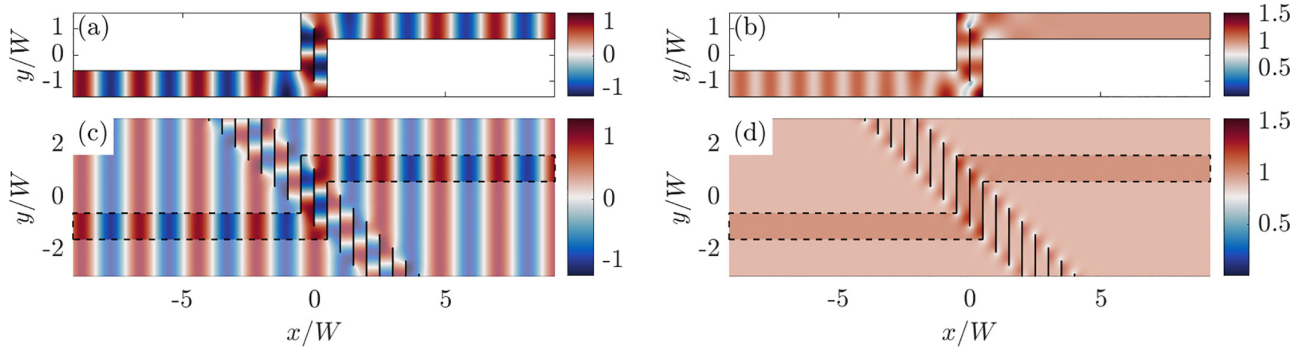

FIG. 11. (a) and (c) real part and (b) and (d) absolute value of the free-surface deformation at $kW = 9\pi/10$. (a) and (b) show the field in a waveguide with one infinitesimally thin plate, while (c) and (d) show the plane wave incidence on a periodic grating made of vertical plates of zero thickness. The grating has a periodicity of $W/2$. The dashed lines indicate where the channel walls would be if we confined this system into a waveguide, and the outer field is slightly masked.

one with a metamaterial made of $N = 5$ plates after the turn, and one with a homogenized medium in its place, using the filling ratio $\phi = 0.9$ that corresponds to $N = 5$ plates. Figure 10 shows the simulated fields as well as the absolute value of r as a function of the frequency for each case. While $|r|$ increases with frequency for the case without plates, it remains mostly constant and near zero for the other two cases (with $N = 5$ plates and a homogenized medium with $\phi = 0.9$), as expected. It should also be noted that there is good agreement between the homogenized model and the field obtained with the plate-array metamaterial. The complex value of $r = r_0 e^{i\varphi}$ for $N = 0$ was used to calculate the reflection coefficient R of the complete system in the 1D model [Eq. (2)].

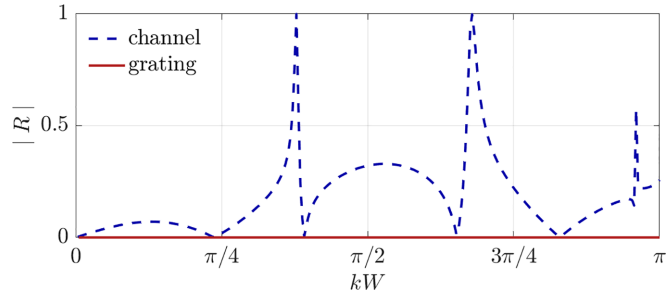

FIG. 12. Numerical result: absolute value of the reflection coefficient for a channel with one vertical plate of zero thickness [Figs. 11(a) and 11(b)] and for a periodic array of plates with zero thickness [Figs. 11(c) and 11(d)].

APPENDIX C: INFINITESIMALLY THIN PLATES

We consider an incident plane wave propagating in a bent channel with one infinitesimally thin plate in the central region, and we compare it with a plane wave incidence on a periodic grating made of infinitesimally thin plates. The grating has a periodicity of $W/2$ to maintain the same distance between plates as in the case of a waveguide.

Figure 11 shows the real part and the absolute value of the free-surface deformation field for a fixed frequency, both in a waveguide and in a periodic medium. Although these two cases might appear similar, there is a difference if we inspect closely in the neighborhood of the plates. The dashed lines in Figs. 11(c) and 11(d) indicate where the channel walls would be if we confined this system into a waveguide. The presence of the channel imposes Neumann boundary conditions on the walls. This confinement leads to a different behavior of the field. In particular, the reflection coefficient for a plane wave incidence in a waveguide is no longer zero as in the case of a periodic grating, as shown in Fig. 12.

[1] K. Y. Bliokh, Y. P. Bliokh, V. Freilikher, S. Savel'ev, and F. Nori, Colloquium: Unusual resonators: Plasmonics, metamaterials, and random media, Rev. Mod. Phys. **80**, 1201 (2008).

[2] T. J. Cui, D. R. Smith, and R. Liu, *Metamaterials* (Springer, New York, 2010).

[3] R. V. Craster and S. Guenneau, *Acoustic Metamaterials: Negative Refraction, Imaging, Lensing and Cloaking* (Springer, New York, 2013).

[4] V. Romero-Garcia and A.-C. Hladky-Hennion, *Fundamentals and Applications of Acoustic Metamaterials: From Seismic to Radio Frequency* (Wiley, New York, 2019).

[5] D. Schurig, J. J. Mock, B. J. Justice, S. A. Cummer, J. B. Pendry, A. F. Starr, and D. R. Smith, Metamaterial electromagnetic cloak at microwave frequencies, Science **314**, 977 (2006).

[6] M. Farhat, S. Enoch, S. Guenneau, and A. B. Movchan, Broadband cylindrical acoustic cloak for linear surface waves in a fluid, Phys. Rev. Lett. **101**, 134501 (2008).

[7] S. Zou, Y. Xu, R. Zatianina, C. Li, X. Liang, L. Zhu, Y. Zhang, G. Liu, Q. H. Liu, H. Chen, and Z. Wang, Broadband waveguide cloak for water waves, Phys. Rev. Lett. **123**, 074501 (2019).

[8] N. I. Landy, S. Sajuyigbe, J. J. Mock, D. R. Smith, and W. J. Padilla, Perfect metamaterial absorber, Phys. Rev. Lett. **100**, 207402 (2008).

[9] V. Romero-García, G. Theocharis, O. Richoux, A. Merkel, V. Tournat, and V. Pagneux, Perfect and broadband acoustic absorption by critically coupled sub-wavelength resonators, Sci. Rep. **6**, 19519 (2016).

[10] E. Monsalve, A. Maurel, P. Petitjeans, and V. Pagneux, Perfect absorption of water waves by linear or nonlinear critical coupling, Appl. Phys. Lett. **114**, 013901 (2019).

[11] F. De Vita, F. De Lillo, F. Bosia, and M. Onorato, Attenuating surface gravity waves with mechanical metamaterials, Phys. Fluids **33**, 047113 (2021).

[12] H. Chen and C. T. Chan, Electromagnetic wave manipulation by layered systems using the transformation media concept, Phys. Rev. B **78**, 054204 (2008).

[13] C. P. Berraquero, A. Maurel, P. Petitjeans, and V. Pagneux, Experimental realization of a water-wave metamaterial shifter, Phys. Rev. E **88**, 051002 (2013).

[14] Y. Xie, W. Wang, H. Chen, A. Konneker, B.-I. Popa, and S. A. Cummer, Wavefront modulation and subwavelength diffractive acoustics with an acoustic metasurface, Nat. Commun. **5**, 5553 (2014).

[15] P. Wei, F. Liu, Z. Liang, Y. Xu, S. T. Chu, and J. Li, An acoustic beam shifter with enhanced transmission using perforated metamaterials, Europhys. Lett. **109**, 14004 (2015).

[16] A. Maurel, J.-J. Marigo, P. Cobelli, P. Petitjeans, and V. Pagneux, Revisiting the anisotropy of metamaterials for water waves, Phys. Rev. B **96**, 134310 (2017).

[17] R. Porter, Plate arrays as a perfectly-transmitting negative-refraction metamaterial, Wave Motion **100**, 102673 (2021).

[18] R. Porter and C. Marangos, Water wave scattering by a structured ridge on the sea bed, Ocean Eng. **256**, 111451 (2022).

[19] B. Wilks, F. Montiel, and S. Wakes, Rainbow reflection and broadband energy absorption of water waves by graded arrays of vertical barriers, J. Fluid Mech. **941**, A26 (2022).

[20] J. Huang and R. Porter, Water wave propagation through arrays of closely spaced surface-piercing vertical barriers, J. Fluid Mech. **960**, A20 (2023).

[21] A. Alù, G. D'Aguanno, N. Mattiucci, and M. J. Bloemer, Plasmonic Brewster angle: Broadband extraordinary transmission through optical gratings, Phys. Rev. Lett. **106**, 123902 (2011).

[22] N. Aközbek, N. Mattiucci, D. De Ceglia, R. Trimm, A. Alù, G. D'Aguanno, M. A. Vincenti, M. Scalora, and M. J. Bloemer, Experimental demonstration of plasmonic Brewster angle extraordinary transmission through extreme subwavelength slit arrays in the microwave, Phys. Rev. B **85**, 205430 (2012).

[23] A. N. Norris and X. Su, Enhanced acoustic transmission through a slanted grating, C. R. Mec. **343**, 622 (2015).

[24] K. Pham, A. Maurel, J. F. Mercier, S. Félix, M. L. Cordero, and C. Horvath, Perfect Brewster transmission through ultrathin perforated films, Wave Motion **93**, 102485 (2020).

[25] Y. He and G. V. Eleftheriades, Magnetoelectric uniaxial metamaterials as wide-angle polarization-insensitive matching layers, Phys. Rev. B **98**, 205404 (2018).

[26] Z. Chu, T. Li, J. Wang, J. Jiang, Z. Zhang, R. Zhu, Y. Jia, B. Gui, H. Zhang, and S. Qu, Extremely angle-stable transparent window for TE-polarized waves empowered by anisotropic metasurfaces, Opt. Express **30**, 19999 (2022).

[27] A. Maurel, S. Félix, and J. F. Mercier, Enhanced transmission through gratings: Structural and geometrical effects, Phys. Rev. B **88**, 115416 (2013).

[28] J. J. Marigo and A. Maurel, Second order homogenization of subwavelength stratified media including finite size effect, SIAM J. Appl. Math. **77**, 721 (2017).

[29] Note that the coordinate system $(\tilde{x}, \tilde{y})$ is rotated by an angle α with respect to (x, y) from Fig. 1, so that the $\tilde{y}$ axis aligns with the interface between the region of the incident wave and the region occupied by the plates.

[30] P. J. Cobelli, A. Maurel, V. Pagneux, and P. Petitjeans, Global measurement of water waves by Fourier transform profilometry, Exp. Fluids **46**, 1037 (2009).

[31] A. Maurel, P. Cobelli, V. Pagneux, and P. Petitjeans, Experimental and theoretical inspection of the phase-to-height relation in fourier transform profilometry, Appl. Opt. **48**, 380 (2009).

[32] A. Przadka, B. Cabane, V. Pagneux, A. Maurel, and P. Petitjeans, Fourier transform profilometry for water waves: How to achieve clean water attenuation with diffusive reflection at the water surface? Exp. Fluids **52**, 519 (2012).

[33] T. Bobinski, A. Maurel, P. Petitjeans, and V. Pagneux, Backscattering reduction for resonating obstacle in water-wave channel, J. Fluid Mech. **845**, R4 (2018).

[34] E. M. Gutiérrez, Experimental study of water waves: Nonlinear effects and absorption, Ph.D. thesis, Université Pierre-et-Marie-Curie (Paris VI), 2017.

[35] J. Hunt, Viscous damping of waves over an inclined bed in a channel of finite width, Houille Blanche **38**, 836 (1952).

[36] C. C. Mei and P. L. Liu, The damping of surface gravity waves in a bounded liquid, J. Fluid Mech. **59**, 239 (1973).